Heavy Flavour in Jets and Azimuthal Correlations

A Senior Project

By

Patrick Steffanic

Advisor, JL Klay

Department of Physics, California Polytechnic University SLO

June 23, 2018

Approval Page

Title: Heavy Flavour in Jets and Azimuthal Correlations

Author: Patrick

Date Submitted: June 10, 2018

Senior Project Advisor: JL Klay

_____

Signature

_____

Date

Contents

1 Introduction

The strong nuclear force, also known as Quantum Chromo-Dynamics(QCD), describes the interactions amongst quarks and gluons, fundamental constituents of matter. There are six different kinds of quarks that QCD describes:up, down, strange, charm, bottom, and top, all bound together by gluons, a force carrying particle. Most normal matter is composed of up and down quarks, things like protons and neutrons. The remaining quarks have only been observed in high energy collisions like those produced at large colliders. These rare quarks are produced in quark–antiquark pairs through various processes. In most situations quarks are always bound together in groups of two or three called hadrons. The particles which are composed of two quarks are called mesons, while the particles composed of three are called baryons. There is a further type of particle which is not composed of quarks called leptons;included in this are electrons, muons, and taus. The existence of quarks and gluons have only been discovered relatively recently. [1] Unlike Quantum Electrodynamics, our most successful particle theory, the force carriers of QCD, gluons, have eight different types. They also can interact with other gluons; compare this to the non-self interacting photon of QED. This results in what some call a quite "messy" theory.

To study QCD we collide particles at high energies in order to "crack" open subatomic particles like protons into quarks and gluons. Protons in the Large Hadron Collider(LHC) have been accelerated to energies of up to 13 TeV in recent years probing what is called the "High Energy Regime." Additionally, experiments like ATLAS and CMS at the LHC have probed the "High Intensity Regime." The LHC has provided three different collision scenarios: proton-proton, proton-Lead ion, Lead ion-Lead ion. Lead is called a Heavy Ion and collisions of this type are largely motivated by studies into the formation of a state of matter called the quark-gluon plasma[QGP] in which quarks that are bound together by gluons have enough energy to separate and move quasi-freely. This state of matter only occurs at high energies and particle densities similar to those found up to a few microseconds after the Big Bang. Studying the QGP could help us to understand key questions about QCD. In particular, such studies could shed light on the nature of quark confinement and chiral phase transitions.

The first experiments that sought to investigate the QGP were performed at the CERN Super Proton Synchrotron(SPS) in the 80s and 90s, with lead ion beams colliding against fixed targets at center of mass energies up to 17 GeV, culminating in indirect evidence of the QGP's existence in 2000. Around

the same time, the Brookhaven National Laboratory's Relativistic Heavy Ion Collider (RHIC) began colliding gold ions at center of mass energies up to 200 GeV. The discovery of jet quenching [2] in those collisions, along with strong hydrodynamic flow, were taken as definitive proof of the creation of QGP. Since then, the experiments at RHIC, and beginning in 2010 at the LHC, have explored the properties of this exotic state of matter. Each year since, the LHC spends a dedicated month of running colliding lead-ions, which the ALICE experiment, uniquely built to measure properties of the QGP, investigates in great detail.

As explained above, QCD is messy and difficult to probe. One way to investigate QCD is by looking at how high momentum constituent quarks and gluons (also called partons), produced through hard-scattering in high energy collisions, interact with the QGP. Hard scattering refers to collisions in which a high transverse momentum transfer occurs between two partons in the incoming nuclei, leading them to be ejected nearly back to back in the transverse plane, traversing the QGP medium and interacting with it. These interactions can elucidate the properties of QCD [4]. Now, the partons that interact with the medium are not observable so we must look at the resulting sprays of particles that are produced when the partons fragment into observable particles. We call these showers of correlated particles "jets" [5]. Jets are an experimentally well studied phenomenon and have been modeled theoretically [6]. Measuring the spectrum of jet energies in proton-proton collisions where it is thought that the QGP is *not* formed provides a baseline for comparisons with heavy ion collisions, where interactions with the medium reduce the energy of the partons before they fragment into jets. This process is called jet quenching and is well documented [7] [8] [9]. Early measurements of jet quenching at RHIC[11] have been confirmed to be qualitatively consistent with new, more precise measurements [13] [14].

To identify the originating parton that resulted in a jet we need some observable connection. If the originating parton is a bottom quark we are afforded a unique signature. A bottom quark produced in the QGP will fragment into a jet containing a bottom meson which has a decay channel that includes at least one lepton (semi-leptonic decay) with an 11% branching ratio. This means that a significant portion of collisions that produce bottom quarks will result in an observable electron with some specific identifying properties that distinguish it from electrons produced from other sources. This method for identifying bottom quark jets in proton collisions is well-established[15] [16]. Additionally there have been studies

from the CDF collaboration at the Fermi National Laboratory Tevatron in heavy flavor properties of bottom quark pairs using a related identification method [17].

These identified bottom jets can provide a probe of the QGP, but first we need to establish a baseline measurement of bottom jets in proton collisions where the QGP is not expected to form. By comparing to this baseline we can establish whether the effects we measure via bottom quark jets are due to the QGP. This study investigates back-to-back azimuthal correlations of high momentum electrons with accompanying hadrons to identify bottom jets decaying semi-leptonically. We also investigate events in which the highest momentum reconstructed jets are led by an electron of similarly high momentum. By looking at the distributions of particles emitted around 180 degrees (the "away side") away from the electron-jet (the "near side") we endeavor to find dynamic jet variables that can reliably and efficiently distinguish jets originating from bottom quarks and those originating from light quarks and gluons. The away side distributions for bottom quark jets should be different from those of light quark and gluon jets. Developing the techniques to measure these differences in proton collisions would provide a probe into potentially significantly different physics than for light quark jets interacting with a QGP produced in heavy ion collisions [23].

2 Theory

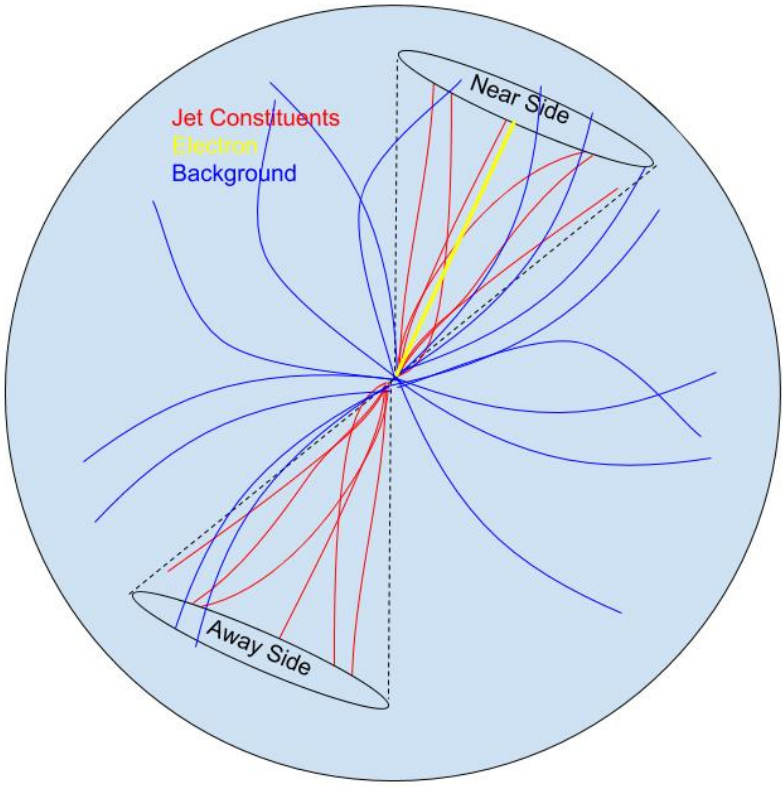

Figure 1: Schematic diagram of a di-jet event.

The following sections outline the formation of QGP in a nuclear collision, the evolution of the QGP, briefly, and the resulting structures pertinent to this analysis.

2.1 Formation and Evolution of the QGP

When two ion beams collide at the interaction point in the center of the ALICE barrel the high energy and high baryon density environment is such that quarks usually bound by the strong force become deconfined. This state of quark and gluon matter is a plasma and has been observed to act like a perfect fluid[10]. The constituents of this fluid are quarks and gluons interacting with each other through QCD processes. For a more detailed treatment of the QGP see [24].

After the initial collision the QGP evolves hydrodynamically before experiencing several phases of what are called "freeze-outs". At a certain temperature the expanding QGP hadronizes, a process by which bare quarks form hadronic pairs or triplets to produce typical hadronic matter; the so-called "hadronic freeze-out" or hadronization. For a small time these hadronic particles are still energetic enough to exchange particles through various interactions. We call the phase in which these hadron-hadron interactions cease the "chemical freeze-out", named so because the hadrons are frozen in a final state at this point. Finally there is the "thermal freeze-out" where no more kinematic interactions occur. The exact details surrounding the various freeze-outs and the temperature and densities at which they occur is still deeply debated and under study. Reference [25] gives an exhaustive overview of what is theorized and known about the QGP and its evolution.

At some point during the evolution of the QGP the hard-scattered partons undergo the process of fragmentation. Similar to hadronization of the softer particles in the QGP, the bare partons convert some of their available energy and momentum into particle-antiparticle pairs that are tightly correlated with the parent parton's original momentum direction, leading to a "jet" of final-state particles. These fragmentation events are probabilistic and produce the hadrons that are measured in the final state of the collision. This leads us to what we actually end up measuring, jets.

2.2 Jets

When hadrons in the LHC are collided at high energies the resulting partons, subnuclear constituents of the collision, come together to form hadrons in a process called hadronization. The highest energy partons result in a collimated conical tree-like spray of particles that we call a jet. The conversion of a free parton into a jet can be characterized by a "fragmentation function". Fragmentation functions, however, cannot be calculated analytically with the standard perturbation theory in QCD, as they become non-perturbative due to energy loss at each successive decay. To sidestep this problem, researchers turn to phenomenological probabilistic ("Monte Carlo") models, like the Lund string model[37], which use measured data to constrain their free parameters, in order to create fragmentation functions that match the observed data which can be used to make subsequent predictions about produced jets.

Jets develop from a single parton, either a quark or gluon, present in the initial collision. This makes jets a natural extension of the partons themselves and an excellent probe into the dynamics of the

collision. Experimentally, however, jets are much messier than the theoretical take suggests. Usually more than one jet or jet pair is produced. It is difficult to reconstruct them completely and uniquely [18], even in proton collisions.

The presence of multi-jet events is ubiquitous in ALICE and the other LHC experiments and are key topological constraints in certain studies including supersymmetry [38] and Higgs searches[39].[1] These multi-jet events, not to mention other compounding factors like jet finder bias and the effects of the underlying event background, can impact the reliability of jet observables.

Nevertheless, the lasting investigation of jets clearly shows their importance in searches for new physics and further development of the Standard Model. The technical challenges of detecting and classifying jets are great but the physics landscape that they enable us to investigate is rich and crucial to our developing an understanding of QCD. The following provide some reviews of jet physics at colliders. [40] [41] [42]

2.3 Jet Quenching in QGP

When the QGP is produced in heavy ion collisions, high momentum partons are produced through hard scattering. As the partons traverse the medium they interact with it through multiple soft scatterings with gluons, losing energy along the way.[19] The energy loss of travelling partons results in a host of consequences. High transverse momentum (p_T) particles are expected to be suppressed relative to proton-proton collisions, since their parent partons have less energy to impart to them, an effect observed at RHIC and the LHC[20]. Additionally, the particles that are produced as the high p_T particles travel will be affected by the energy loss.[21]

The Relativistic Heavy Ion Collider(RHIC) first observed jet quenching effects in Au+Au collisions; a strong indication for the existence of QGP at the time. Subsequent observations of jets in deuteron-Au collisions established that the observed quenching was not due to "cold nuclear matter" effects[22] and solidified the evidence that QGP is created in heavy ion collisions. Since that time the LHC has been observing jet quenching in Pb-Pb collisions at higher center of mass ($\sqrt{s}$) energies than those at RHIC.

[1] As the researcher in [39] points out, though, the presence of multiple jets serves as a background in that study.

2.4 Quark and Gluon Jets

As mentioned earlier, initial state particles like quarks and gluons interact with the medium through multiple scatterings and radiation. In theory, one can unambiguously assign a jet to its initial state particle, enabling us to distinguish quark from gluon jets. Experimentally, however, finding a way to isolate pure samples of either reliably is challenging, but would help tremendously in our investigations of QCD and in the search for new physics. In supersymmetry, for example, "sparticles", the so-called supersymmetric partners of the conventional particles, are expected to predominantly produce quark jets while gluon jets represent background processes. Having a pure quark jet sample and comparing its properties to theory would be critical to discovering sparticles. In [33] the authors outline the more technical aspects of quark versus gluon jets for different event types. In that paper quark jets originating from up, down, and strange quarks are considered. In the study presented in this paper, our attempts to identify bottom-quark led jets ("b-jets"), provides a means to study the physics of quark jets.

Interestingly, b-jets have been observed to be quite a bit more like gluon jets than quarks jets. The OPAL collaboration [34] found that b-jets contained more charged particles over a wider area than light quark jets(uds), similarly to gluon jets. This could pose a difficult problem for distinguishing bottom jets from gluon jets when one uses the hadronic decay channel for B-mesons to identify the bottom quark jets. One solution is to apply kinematic cuts on bottom mesons with long decay lengths to tag b-jets based on early decay products. For our study we require the presence of a high-p_T electron in conjunction with a jet, which should suppress some of the background. We do not currently apply kinematic cuts but that is worthy of further investigation.

Most experimental investigations into differences between light quark and gluon jets have been done at colliders such as LEP, which collide beams of electrons that produce pure quark-anti-quark pairs or gluons that fragment into jets. These studies focus on differences between the color factors of quarks and gluons and are nicely summarized in [35]. Lately, more theoretical work has been done simulating key jet observables and topological configurations that would help discriminate light quark and gluon jets. In [33] the authors simulated many different jet configurations: 2-jet, 3-jet, γ-jet, b-2jet, and others. They investigated the effect of kinematic cuts on light quark jet and gluon jet purity. The authors found that one can get 90% pure gluon jets in 3 jet events. Further work by Havard [36] investigated an exhaustive

list of existing and newly developed jet observables in Monte Carlo simulations for differences between quark and gluon jets. They found that with a multivariate approach a 95% gluon jet reduction could be attained with 50% light quark efficiency, meaning that they could reliably tag light quark jets at reasonable efficiency with minimal contamination from falsely identified gluon jets. They also found that the same could be achieved with just two observables: charged particle multiplicity and p_T-weighted linear radial moment (jet "girth"). When considering differences between bottom quark and gluon jets, however, this is somewhat unhelpful as it has been observed that bottom quark jets have similar charged particle multiplicities and girths, though [34] shows a slight difference. Very little work has been done comparing bottom jets and gluon jets beyond [34].

Most of this work shows that novel observables or kinematic cuts will be required to truly discriminate bottom jets from gluon jets. That said, it is important to investigate bottom quark jets compared to "inclusive" jets, that is, all jets *not tagged by an electron*, first.

3 Experiment

We will now briefly describe the experimental setup in place for studying jets with the ALICE detector at the LHC.

3.1 Large Hadron Collider

The Large Hadron Collider[26] is the largest of many experiments operated by CERN, the European Organization for Nuclear Research. It consists of a 27 kilometer long ring of superconducting magnets designed to collide two hadron beams traveling in opposite directions. Currently, it collides proton beams at a center of mass energy of 13 TeV. Figure 2 shows the accelerator complex and its components. The LHC collided proton beams at a center of mess energy of 7 TeV in 2012. The LHC has also collided lead ions at a center of mass energy of 2.76 TeV per nucleon in recent years.

Around the ring are six detectors, ALICE[26], ATLAS[26], CMS[27], LHCb[27], LHCf[27] and TOTEM[27]. The ATLAS (A Toroidal LHC Apparatus) and CMS (Compact Muon Solenoid) experiments are general purpose physics detectors exploring topics from Higgs boson detection to new particles and extra dimensions. The LHCb (Large Hadron Collider Beauty) experiment is concerned with studying matter/antimatter differences using primarily bottom quarks due to their high precision. ALICE

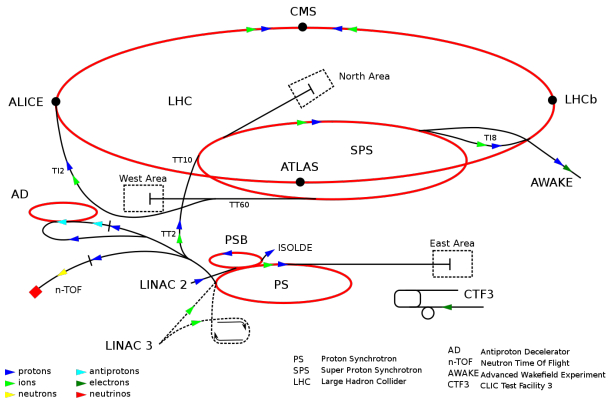

Figure 2: A schematic layout of the LHC acceleration chain and detectors on the ring

(A Large Ion Collider Experiment) is a heavy-ion detector designed to study the quark-gluon plasma. LHCf and TOTEM are small, specialized experiments investigating topics like forward physics.

3.2 A Large Ion Collider Experiment

ALICE is a heavy-ion detector on the LHC ring designed to study the quark-gluon plasma, a high energy, high density form of matter created when heavy ions are collided at high center of mass ($\sqrt{s}$) energies. Unique to ALICE is its excellent particle identification and tracking capabilities over a large momentum range near the center of the collisions, called mid-rapidity. The Time Projection Chamber (TPC) provides excellent tracking and momentum information especially in the low momentum region due to a low magnetic field of 0.5 T permeating the entire detector. This is supplemented by tracking information from the Inner Tracking System (ITS), a group of six silicon tracking detectors employing three separate methods that give very precise track location and origin information. Furthermore, the Transition Radiation Detector (TRD) provides electron identification and the Time Of Flight (TOF) detector provides particle identification for charged hadrons of intermediate momentum (up to a few GeV). Finally, ALICE boasts an Electromagnetic Calorimeter (EMCal) which, in addition to extending the momentum range, aids in the study of jet quenching. The EMCal enables triggering on high p_T jets and improves the jet energy resolution.

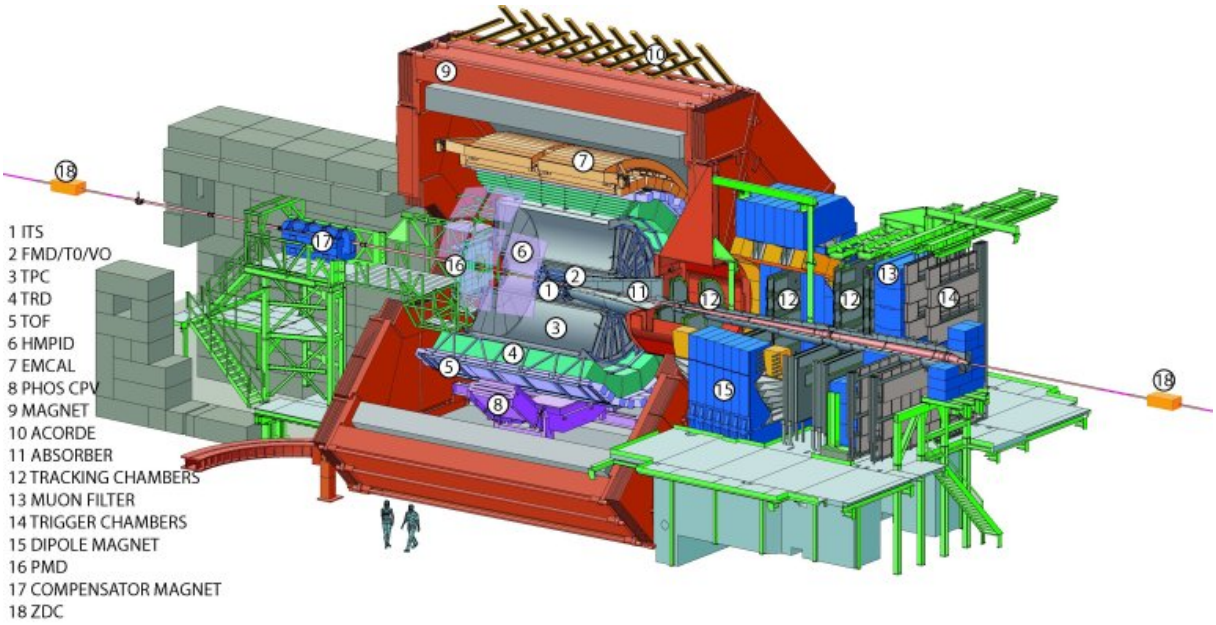

Figure 3: Schematic cutaway of the ALICE detector indicating its many subsystems.

3.3 ALICE Detector Subsystems

The ALICE detector is composed of a central barrel and a forward muon arm consisting of 15 detector subsytems. Figure 3 shows a schematic of the detector. The LHC provides collisions at the middle of the ALICE central barrel at what's called the Interaction Point (IP). In addition to the detectors, the ALICE experiment has designed a fast triggering system that provides crucial data collection decision making capability to enable ALICE to study rare processes. This paper will outline the most important detectors for our analysis.

3.3.1 Triggering

Particle collisions occur in short windows and in order to record them without collecting large amounts of empty data ALICE employs a triggering system [28]. At the most basic level a trigger is an indication that an event of interest has started that percolates through the subsystems telling every detector to start recording. This signal can be sent as fast as 1.2 μs after an interaction is detected. The first level trigger detectors are the T0 and V0, as they are closest to the interaction point. There are also "high-level" triggers which provide a reduction to the recorded data volume by selecting more interesting physics. In

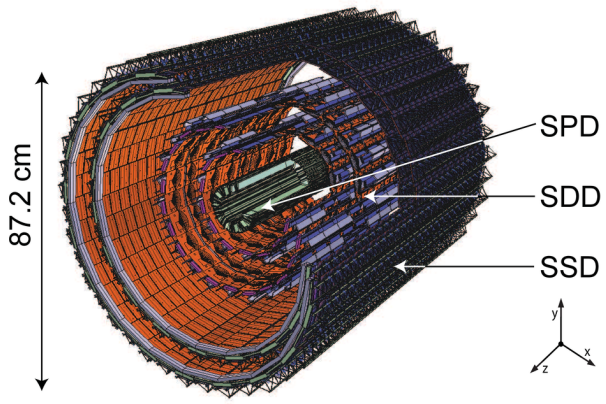

Figure 4: Schematic drawing of the ITS indicating the location of the Silicon Pixel, Silicon Drift, and Silicon Strip detectors

this analysis, we use the EMCal jet trigger, which is one of these high-level triggers, to select events with jets as well as to extend the range of jet energies we can measure.

3.3.2 ITS

The innermost barrel subsystem is the Inner Tracking System (ITS) [29], shown in Fig.4 which is comprised of three individual subsystems: Silicon Pixel Detector (SPD), Silicon Drift Detector (SDD), and Silicon Strip Detector (SSD). Each subsystem within the ITS consists of two-layers and operates on different physical principles. The Silicon Pixel Detector comprises the first two layers nearest to the interaction point. When the collision occurs between the two beams they are not always perfectly aligned and so we measure the overlap using a parameter called the impact parameter. The SPD provides good impact parameter resolution and, with help from the Forward Multiplicity Detector (FMD), the charged particle multiplicity. The second two layers are the Silicon Drift Detector followed by the last two, the Silicon Strip Detector. These last four layers provide further tracking information close to the interaction point and particle identification via energy loss (dE/dx). As a whole, the ITS provides tracking information near the vertex, primary vertex measurements, and particle identification from energy loss.

3.3.3 TPC

The Time Projection Chamber (TPC) is the main tracking detector in the ALICE central barrel[30]. The TPC is a large volume barrel detector filled with a neon-based gas mixture. The gas is embedded in a

uniform high-voltage electric drift field that attracts electron clouds from ionized particles toward end plates covered in about 560,000 individual detector elements (pads) to provide position information in the x and y directions. The drift time can be used to provide z axis information and the particles can be accurately tracked on their pathway through the detector volume. The TPC provides excellent tracking and momentum information with a good momentum resolution. Particle identification over a large momentum range is achieved via the energy loss of particles through ionization as they travel through the TPC volume. The specific ionization energy loss is provided through the Bethe-Bloch formula which has the following parameterized form:

$$\frac{dE}{dx}(\beta\gamma) = \frac{P_1}{\beta^{P_4}}\left(P_2 - \beta^{P_4} - ln\left(P_3 + \frac{1}{(\beta\gamma)^{P_5}}\right)\right), \tag{1}$$

where β is the particle velocity, γ is the relativistic factor, and P_{1-5} are fit parameters. Figure 5 shows the measured energy loss as a function of particle momentum in the TPC. Each solid black line represents the parameterization for distinct particle species. We see that in certain momentum regions there is clear separation between different particle species. This allows us to identify different particles in the detector volume. For example, in this analysis we identify electrons using the TPC along with the other detectors.

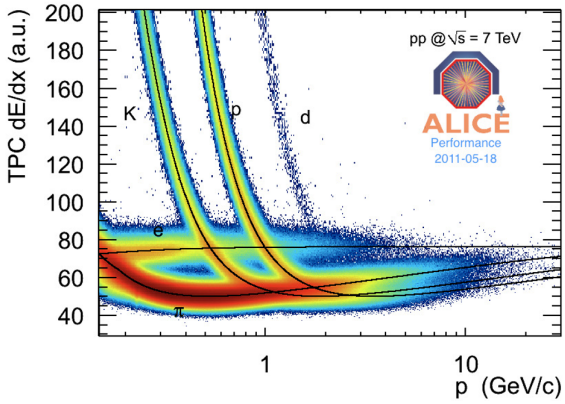

Figure 5: The specific ionization energy loss vs. transverse momentum in the TPC. The letters indicate each particle species and each black line represents the parameterization for that species.

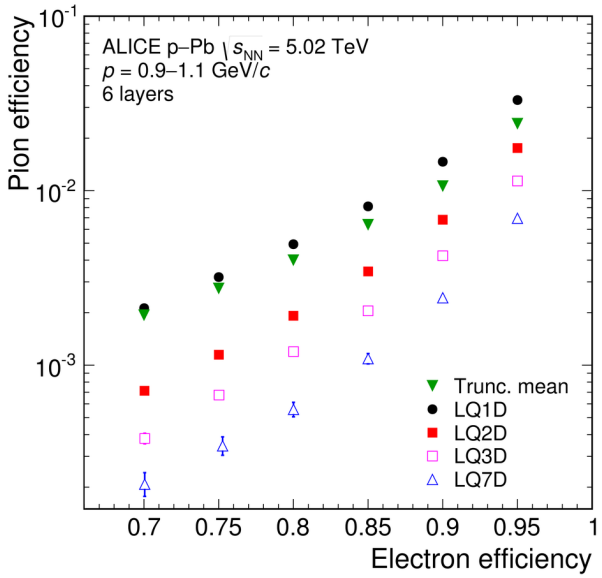

Figure 6: Electron identification efficiency in the TRD as compared to pion selection efficiency for various methods of combining signals from each radiator. Pion rejection, or the likelihood that the detector correctly identifies a pion and rejects it, is one over the pion efficiency.

3.3.4 TRD

The Transition Radiation Detector (TRD) provides electron identification and high momentum triggering for the ALICE experiment[31]. The TRD consists of six layers of radiators stacked radially in the outer barrel, along with gaseous drift regions and readout chambers. When a high momentum particle transitions from one type of material to another a photon is emitted whose energy is, on average, proportional to the Lorentz factor γ of the incident particle. This provides excellent discrimination between electrons and pions, pions being the lightest meson and most ubiquitous particle that we detect in collisions, moving through the TRD's volume. Each layer provides an individual measurement of the transition radiation which, when combined across all the radiators, provides a likelihood that the incident particle is an electron through Bayesian inference. Other methods like a simple average and neural networks have been used to identify electrons as shown in Figure 9.

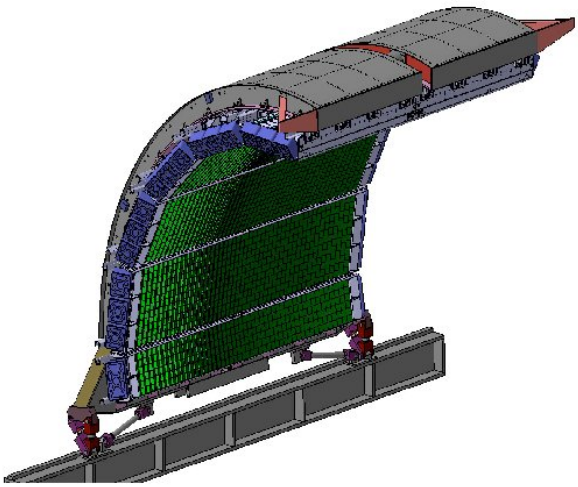

Figure 7: A schematic view of the EMCal modules.

3.3.5 EMCal

The Electromagnetic Calorimeter (EMCal) is a lead-scintillator sampling calorimeter detector that measures jet energies across a wide range as well as providing a jet trigger[32]. The main goal of the EMCal is to measure jet quenching by detecting a large portion of a jet's energy as well as providing a fast and efficient jet trigger which increases the statistics of event samples for studying jet observables. The EMCal is composed of many lead-scintillator towers coupled to fiber optics which deliver the scintillated light produced by electromagnetic showers to readout modules. By coupling the energy measurements of the EMCal and the TPC momentum measurements we can provide electron identification due to the fact that electrons deposit all of their energy into the EMCal whereas hadrons only deposit some portion. Recently another calorimeter, the Di-Jet Calorimeter (DCal), has been installed opposite to the EMCal to measure back to back jet energies. While the analysis presented here does not use the DCal, the EMCal is indispensable in this analysis as it provides access to the complete jet composition and energy profile, increases our energy range with excellent resolution, and provides electron identification across a wide energy range.

4 Data and Analysis

Over the course of the work done for this project, we focused on two analyses. The goal of both analyses is to investigate bottom quark jet effects, but for the first analysis we focused on identifying electrons from semi-leptonic decays in the EMCal detector and producing an azimuthal correlation plot with hadrons in the whole detector acceptance. For the second analysis, an extension of the first, we attempted to include full jet reconstruction with our identified electrons to compare jets originating from heavy quarks to those originating from light quarks and gluons. In order to do this, a way to discriminate the two jet populations was devised and several variables pertaining to the jets' qualities were calculated.

We use two trigger conditions across both analyses. The first is simply minimum bias conditions which is defined by particle hits in the T0 and V0 detectors, considered the minimum interaction required to signify a collision. Additionally we use any event satisfying an energy threshold in the EMCal to extend our energy range.

The electron-hadron azimuthal correlations analysis consisted of several steps, each outlined in the following sections: electron identification, hardonic and photonic electron background estimation, mixed event analysis, and raw and corrected correlations. Electron identification was performed using the combined signal of several detectors to produce a sample of electrons. The population was then put through a set of kinematic cuts to select mostly electrons from semi-leptonic decays. This sample consists mostly of electrons from semi-leptonic decays, but also contains some contamination due to hadrons as well as electrons from photonic conversions in the detector volumes.

To estimate the hadronic background we selected a population containing no leptons and produced for that population a histogram of the ratio of the energy desposited in the EMCal with the momentum measured in the TPC. By comparing the distribution of this population with that of our semi-leptonic electron population we determined the percent hadronic contamination in our population. This is outlined in further detail later in this paper. In order to measure the contamination due to photonic electrons within our population we constructed pair-wise invariant mass and opening angle plots. Electrons originating from photonic conversions inside the detector volume will come in a pair, oppositely-signed with a small opening angle between them. The population of oppositely-signed pairs of electrons with small opening angles, a subset of the total semi-leptonic electron population, provides a percent photonic electron

contamination.

With the above population of semi-leptonic electrons we produced an azimuthal correlation plot with all the hadrons in each event. Due to the requirement that our electrons appear only in the EMCal we have introduced a bias into our calculation. In order to correct for geometric acceptance we performed a so-called mixed event analysis. The method takes our semi-leptonic electron population and correlates them with all hadrons from events to which the electrons do not belong. This gives us a mixed event electron-hadron azimuthal correlation plot. To produce the final corrected semi-leptonic electron-hadron azimuthal correlation plot we took the ratio of the uncorrected plot with the mixed event plot.

The second analysis looks at full jets (ones with both their charged and neutral constituents accounted for) in the EMCal that originated from a heavy quark (as tagged by the presence of a high-p_T electron) and full jets originating from all other sources (those not tagged with a high$-p_T$ electron). These jets are the "near-side" jets, used only to tag b-jet pair candidates, while the "away-side" jets, emitted nearly back to back, are used to compare b-quark tagged and untagged jet properties. To determine that the full jets have likely originated from a heavy quark we look for near-side jets with an electron as its leading constituent. The ALICE software provides a probable PID signal using all PID detectors for each track; we used this to identify the electrons. If there is more than one near-side jet in the event we chose the one with the highest jet p_T. Then, if the near-side jet is not electron-led, we suppose that it originated from a light quark or gluon which we will refer to as "inclusive".

In order to compare jets originating from light quarks and gluons with one originating from a heavy quark we look for jets that are traveling in nearly opposite directions. The jet traveling opposite of the full jet is called the away-side jet. Since there is no EMCal coverage on the away-side, we only reconstructed charged jets on the away-side. We required that the away-side jet axis lie within $\frac{\pi}{4}$ of the axis opposite that to the near-side jet. If a near-side jet has a partner away-side jet, as described above, we called that a back to back event. These back to back events should be indicative of the near-side and away-side jets originating from hard scatterings of pair-produced partons. The away-side jets likely originate from the same type of (anti-)parton as the near-side so we may compare them. Using the near-side as the tag and studying the away-side with minimal constraints hopefully eliminates or reduces the selection bias that our triggering and analysis cuts impose on the near-side jets.

Once we identified the back to back events we constructed many kinematic variables for each away-side population (electron-led near-side and inclusive near-side). We compared the populations over several large p_T ranges by taking their ratios. The kinematic variables investigated were mostly inspired by studies of the differences between jets originating from light quarks and those originating from gluons at LEP and elsewhere [35], [36]. We found that, with our level of heavy flavor jet purity and statistics, most of the kinematic variables investigated provided little to no discriminatory power between jets originating from heavy quarks and the inclusive population.

4.1 Electron PID

An integral piece of measured semi-leptonic decay from bottom mesons is identifying high-momentum electrons. Many analyses within ALICE have investigated electron identification for semi-leptonic decays and so we apply a series of standard cuts shown in Table 1. These cuts are used in other similar analyses, see [12].

Cut	Value
TPC Refit	True
ITS Refit	True
XY Max DCA	$0.0182 + 0.0350/p_T^{1.01}$ cm
Z Max DCA	2 cm
Max χ^2 per ITS Cluster	36
Max χ^2 per TPC Cluster	4
Min # of TPC Clusters	80
Min # of ITS Clusters	3
p_T Range	> 1 GeV
Require Hit in Both SPD Layers	True
Accept Kink Secondaries	False

Table 1: Standard heavy flavor cuts.

This analysis required a robust identification of electrons using combined signals from many detectors. We employed three detectors for our primary electron identification: the TPC, TRD, and EMCal. Each provides a different momentum phase space which allowed us to identify electrons across a wide momentum range. The TPC provides fractional energy loss vs. momentum which is subtracted from the Bethe-Bloch curve for electrons to provide an electron likelihood distribution. The TRD was designed to provide electron detection and so an electron likelihood is provided through its software library. The

EMCal provides a direct measurement of the particle's energy and it is compared to the momentum measured by the TPC; electrons are expected to deposit almost all of their energy into the EMCal resulting in an E/p_T distribution centered around unity. The effectiveness of each pair of cuts shown in Table 2 is indicated in the following section, with the resulting distribution in the third detector compared to that detector's cuts.

Detector Cut	Lower Bound	Upper Bound
TPC dE/dx	-2σ	+2σ
TRD $e-$ likelihood	80%	100%
EMCal E/p_T	.85($\leq$ 6 GeV), .95($\geq$ 6 GeV)	1.15($\leq$ 6 GeV), 1.25($\geq$ 6 GeV)

Table 2: The cuts applied to each detector's particle signal.

The TPC takes advantage of the energy loss that occurs as a charged particle moves through a gas, as governed by the Bethe-Bloch equation. Figure 5 shows the ALICE standard TPC fractional energy loss vs. momentum distribution along with the Bethe-Bloch curves for particle energy loss superimposed. After applying the EMCal and TRD cuts we plotted the resulting TPC electron likelihood obtained by subtracting the Bethe-Bloch energy loss distribution from the fractional energy loss. This plot with the TPC cuts superimposed is shown in Figure 8.

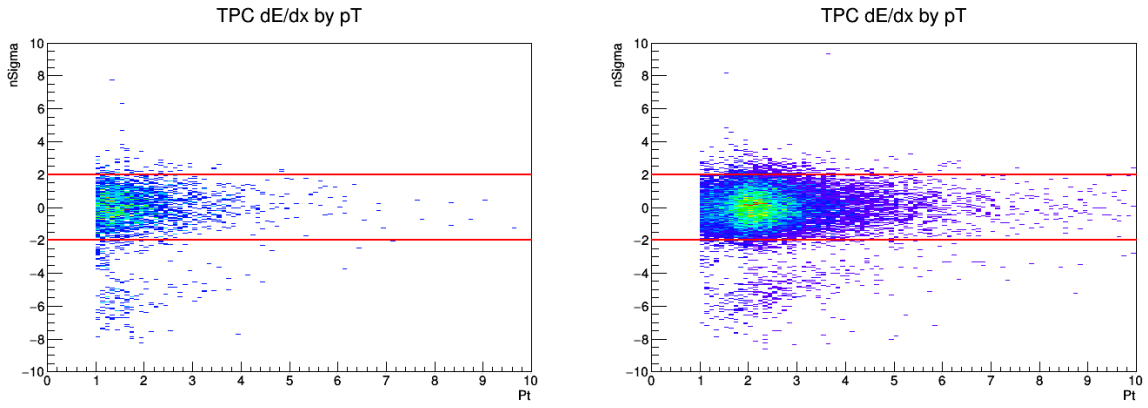

Figure 8: TPC dE/dx distribution of candidate electrons after applying EMCal PID cuts and TRD PID cuts. The left plot shows Minimum Bias (MB) data, the right plot shows EMCal triggered data. Because of our requirement that electrons reside in the EMCal, the EMCal triggered data greatly enhances statistics. Red lines indicate a $\pm$ 2 σ acceptance according to the Bethe-Bloch curve for energy loss through a medium.

The TRD uses transition radiation to identify electrons. It is particularly suited to identify electrons as the probability of transition radiation occurring is increased by a factor of γ, and the electrons will have the highest γ of any charged particle with a particular momentum in any given event due to their light mass. The TRD software package provides a likelihood measurement for identifying electrons. We applied the TPC and EMCal cuts in Figure 9 and superimposed an 80% likelihood cut.

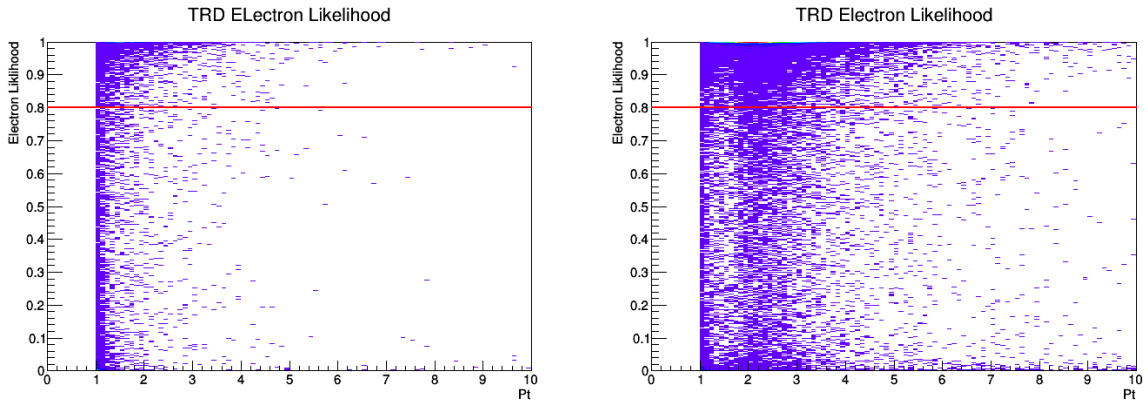

Figure 9: TRD likelihood plot of candidate electrons being consistent with an electron hypothesis after applying EMCal PID cuts and TPC PID cuts. The left plot shows Minimum Bias (MB) data, the right plot shows EMCal triggered data. In addition to boosting statistics, the EMCal triggered data allows us to extend our p_T range far beyond MB data. Red lines indicate an 80% likelihood that a given particle is an electron.

The EMCal measures energy deposited in its detector volume by particles. Electrons are expected to deposit most of their energy into the EMCal in a tight cone, whereas hadrons are expected to deposit only some of their energy in a wide, messy cone. Cuts on the shape of the electromagnetic shower can exploit the shape difference. For our analysis, we compared the total energy deposited into the EMCal with the momentum measured in the TPC for EMCal clusters matched to TPC tracks. We applied the TPC and TRD cuts and plotted the resulting distribution in the EMCal for several momentum ranges. This is shown in Figure 10 with a cut superimposed for each momentum bin.

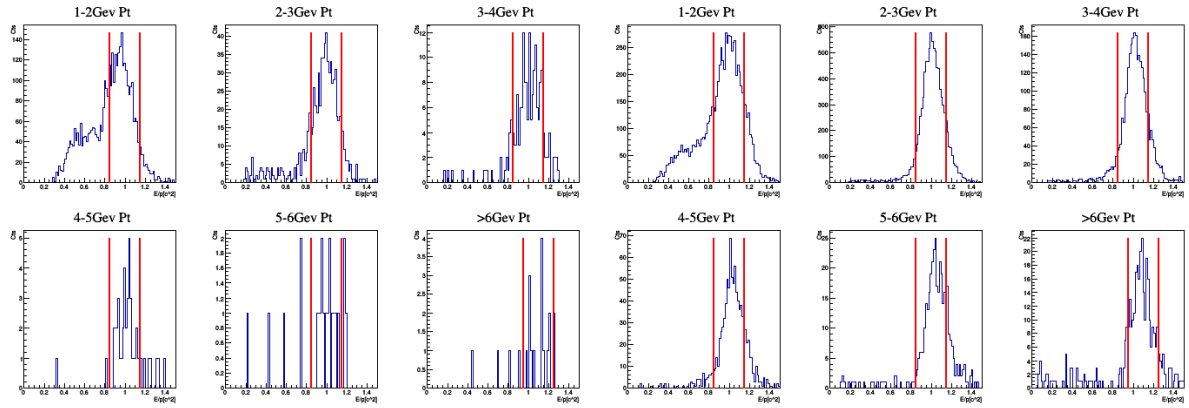

Figure 10: Ratio of the Energy deposited in the EMCal over p_T measured in the TPC of candidate electrons after applying TRD PID cuts and TPC PID cuts. The left six panels show Minimum Bias (MB) data, the right six panels show EMCal triggered data. Each individual plot represents a momentum bin for our candidate electron. Electrons deposit most of their energy in a small electromagnetic shower resulting in an energy-momentum quotient of $\sim$1. Red lines indicate a selection criteria between .85 and 1.15 for electrons with $p_T < 6$ Gev and between .95 and 1.25 for those with $p_T > 6$ Gev.

Sometimes parameters are not measured for certain particles due to insufficient signals in PID detectors. In order to determine which detectors limit our statistics the most we plotted the number of rejected particles for each detector. This is shown in Figure 11.

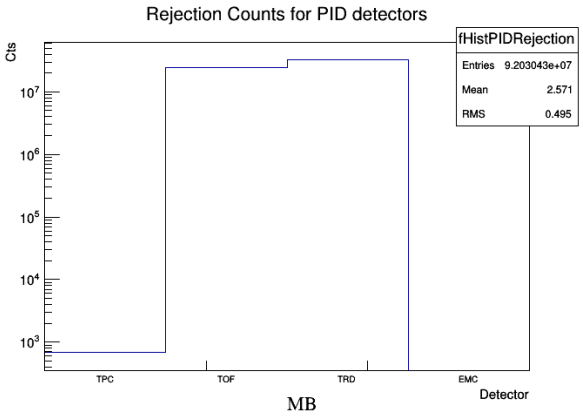

Figure 11: Rejection statistics per detector for candidate electrons in both MB and EMCal triggered data.

After applying all three cuts (TPC, TRD, EMCal) we were left with a distribution of mostly electrons. To better understand the number of electrons passing our cuts in any given event we counted the electrons per event and plot the distribution in Figure 12.

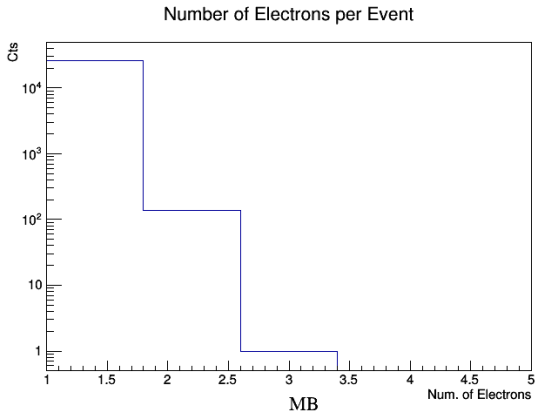

Figure 12: Number of candidate electrons per event. Events with zero electrons not shown. Note also that the area under the plot represents the total number of events with candidate electrons.

4.2 Background Estimation

In order to determine the purity of our electron sample we had to measure the background. Our background consists chiefly of misidentified pions and electrons from photon conversions in the detector structure. We took advantage of the TPC fractional energy loss to select pions and applied the EMCal E/p_T distribution to determine the overlap with the electron cuts. We applied kinematic cuts on the electrons from photon conversions due to the fact that a photon striking the detector structure will always produce an electron-positron pair with low invariant mass and low opening angle. When we compared the invariant mass and opening angle distributions of like-signed electron pairs to that of unlike-signed electron pairs we were able to make cuts to reduce contamination from photon conversion pairs.

Figure 13 shows the EMCal E/p_T distribution for pions selected by the TPC. Superimposed are the cuts applied to select electrons as described in the previous section. This provided us with a measurement of how many pions are contaminating our electron sample.

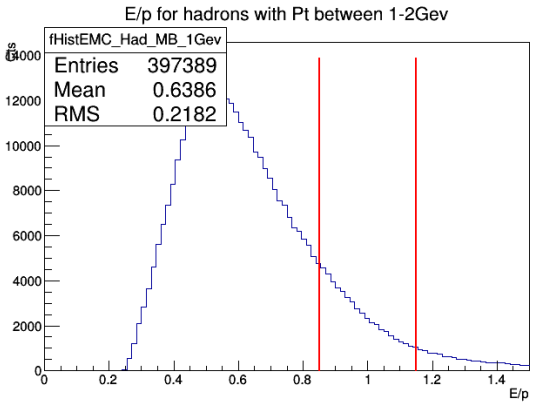

Figure 13: Hadronic E/p_T distribution in MB data for hadrons with 1 Gev $< p_T <$ 2 GeV/c. The red lines show the region selected for electron candidates.

Figure 14 shows the invariant mass distributions and opening angle distributions for like-signed and unlike-signed electron pairs. Superimposed is the cut below which particles are considered photon conversion pairs. We applied a $<$ 0.1 GeV/c^2 cut on the electron pair invariant mass and $<$ 0.1 rad on the opening angle between the pairs. The peaks within these cuts represent the photon conversion pair population.

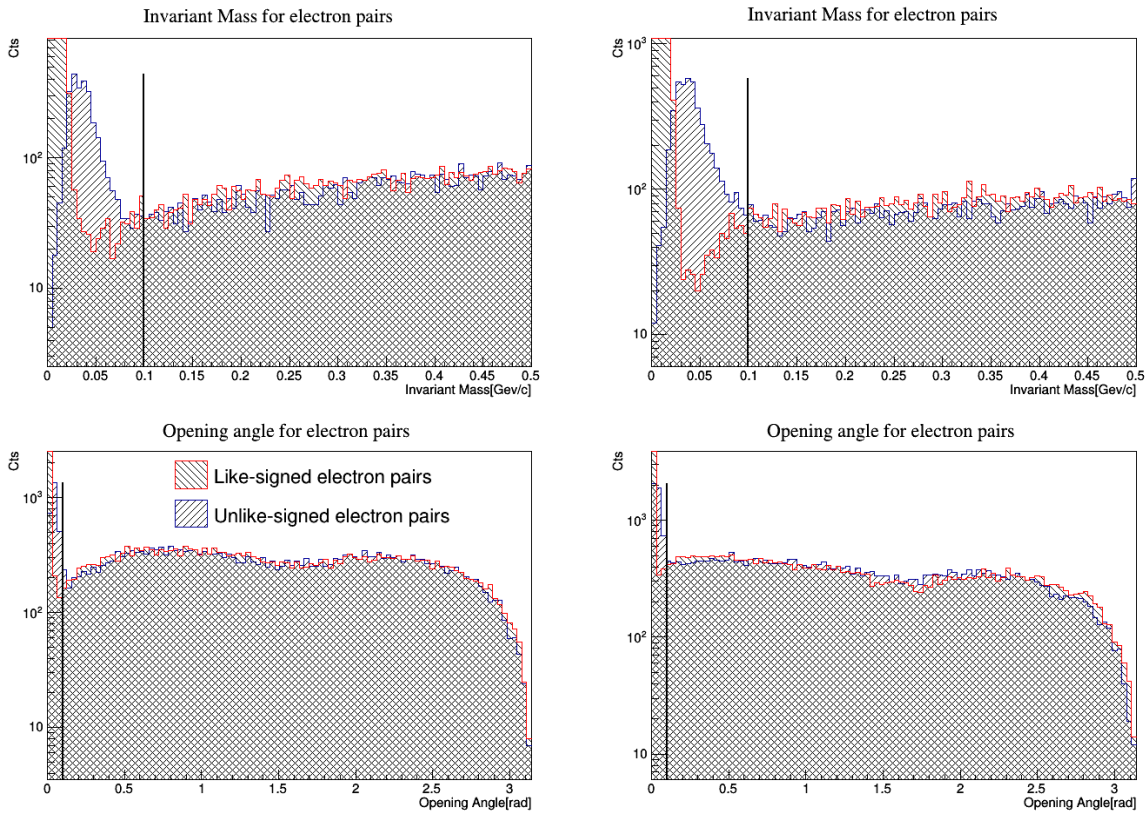

Figure 14: The invariant mass (top) and opening angle (bottom) of all pairs of like-signed (red) and unlike-signed (blue) electron pairs. The left plots show the MB data and the right plots show EMCal triggered data. The black line indicates that below 0.1 GeV/c^2 the peak in the blue distribution represents potentially pair-produced electrons later in the detector volume.

We compared our original electron population to those selected with this cut and counted the number that belong to both populations. This misidentification is represented in Figure 15 as the total number of electrons that reside in both populations from all our events.

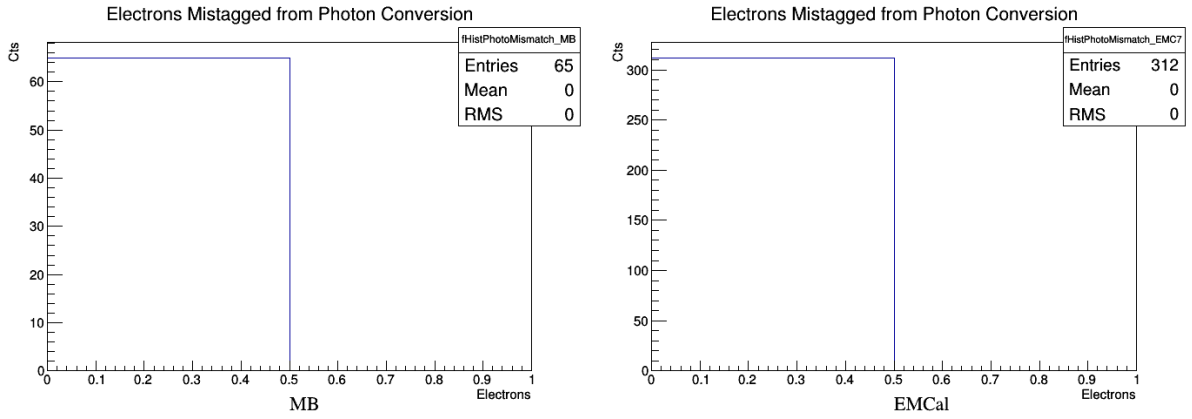

Figure 15: The number of electrons from our candidate electron sample that lie within the cuts for invariant mass and opening angle. The left plot shows MB data and the right plot shows the EMCal triggered data. About 3% of our candidate electron sample also falls into the conversion-pair electron sample.

4.3 Azimuthal Correlations

With a relatively pure high-p_T electron sample, we correlated each electron with the hadrons remaining in the event. We first created several transverse momentum bins for the electrons and the correlated hadrons; these are summarized in Table 3.

Tagged Electron	Correlated Hadrons
1-2 GeV/c	0.3-1 GeV/c
2-4 GeV/c	1-2 GeV/c
4-8 GeV/c	2-4 GeV/c
	4-8 GeV/c

Table 3: Transverse momentum (p_T) bin ranges for the tagged electron and hadrons correlated with it.

We plotted the difference in azimuthal angle, $\Delta\phi$, between each electron and each hadron in every event. We expect a peak around 0 rad and π rad representing the back to back jets that are produced from the initial hard-scattering. Figure 16 shows the correlations for Minimum Bias events. In each we see the hallmark double peak structure.

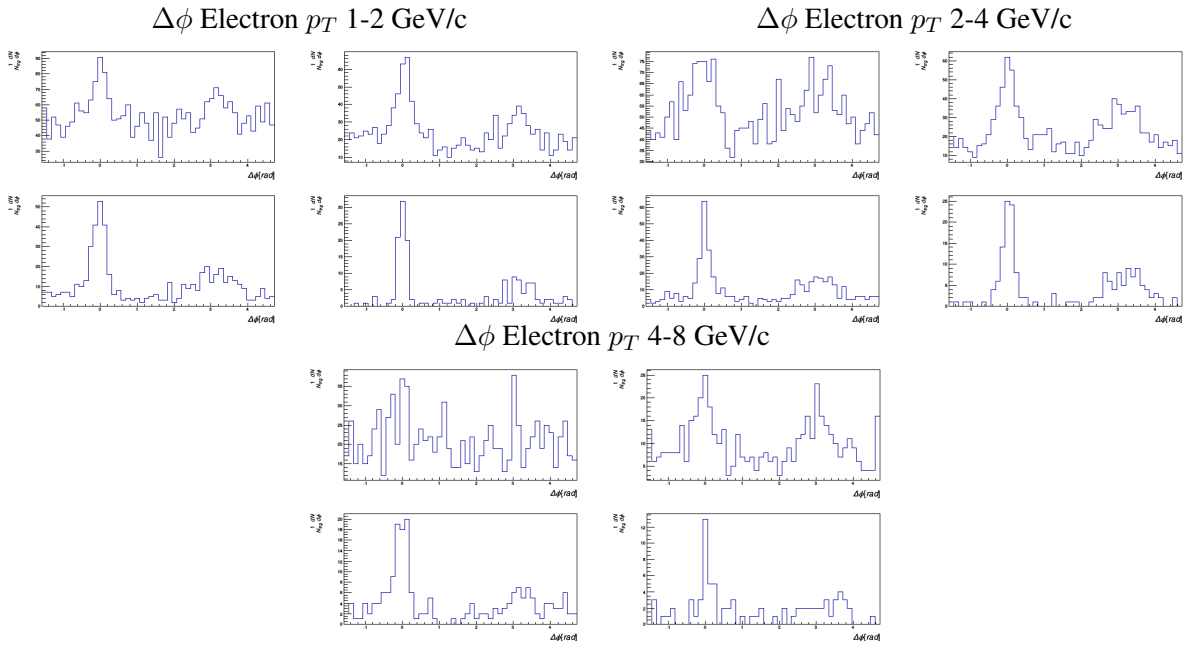

Figure 16: Raw azimuthal correlations of candidate electrons and all other hadrons in that MB event. Each group represents a candidate electron p_T bin: 1-2 GeV/c (top left), 2-4 GeV/c (top right), and 4-8 GeV/c (bottom). Each individual plot in a group represents an associated hadron p_T bin: .3-1 GeV/c, 1-2 GeV/c, 2-4 Gev/c, 4-8 Gev/c. A clear double peak structure is evident in some p_T bins. By comparing this to the Mixed Event correlations, one might attribute this as an effect of limiting the acceptance for trigger particles by the EMCal acceptance.

4.4 Corrected Correlations and Mixed Event Analysis

In order to correct for geometrical bias in our analysis we use a Mixed Event method. This method requires that we compute the $\Delta\phi$ for each electron with the hadrons of events to which it does not belong. The resulting distribution should be uniformly distributed if there are no geometrical biases present. We then subtract that distribution from the correlations in Figure 16, the uncorrelated background. Our Mixed Event Analysis reveals a large bias around the EMCal volume due to our requirement of using the EMCal as a PID detector. Figure 17 shows the $\Delta\phi$ for the uncorrelated mixed event hadrons. Figure 18 shows the corrected azimuthal correlations for our electron sample and their event's hadrons. We note that the corrected correlations don't show the signature double peak quite as clearly, indicating that the structure in the raw distributions may have been due to detector bias.

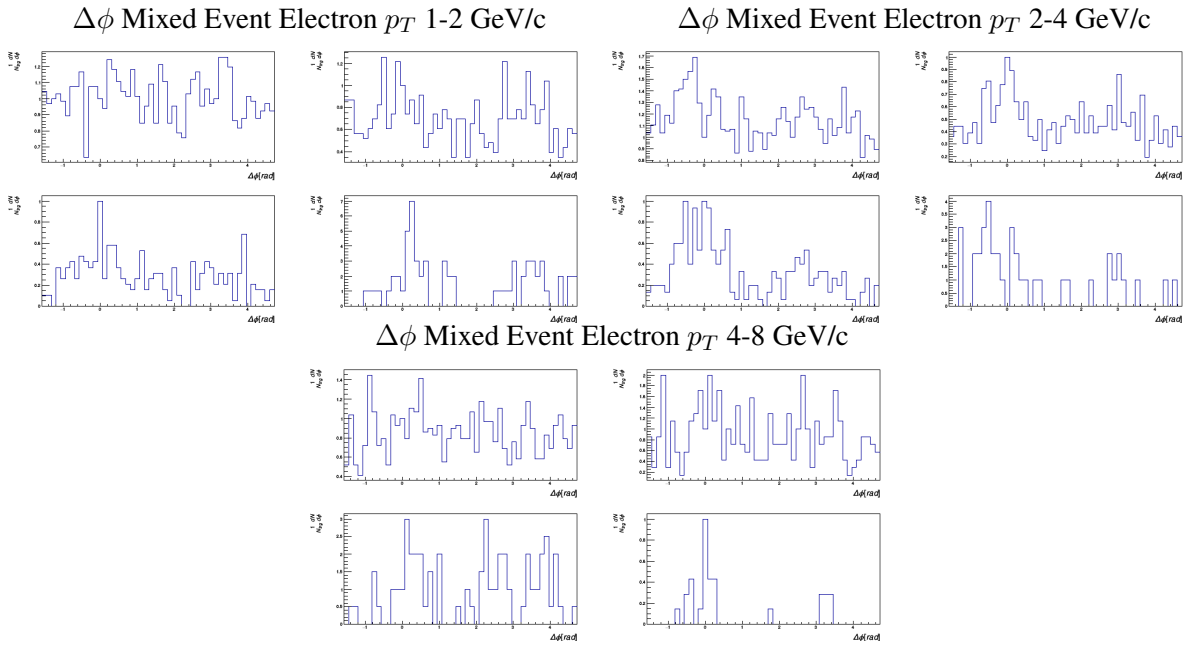

Figure 17: Mixed event azimuthal correlations of candidate electrons and all other hadrons in other MB events. Each group represents a candidate electron p_T bin: 1-2 GeV/c (top left), 2-4 GeV/c (top right), and 4-8 GeV/c (bottom). Each individual plot in a group represents an associated hadron p_T bin: 0.3-1 Gev/c, 1-2 Gev/c, 2-4 Gev/c, 4-8 Gev/c. These plots correct for the geometrical detector acceptance bias. The enhancement lies within the EMCal acceptance and falls off rapidly indicating that a "good" mixed event correlation requires 2π acceptance.

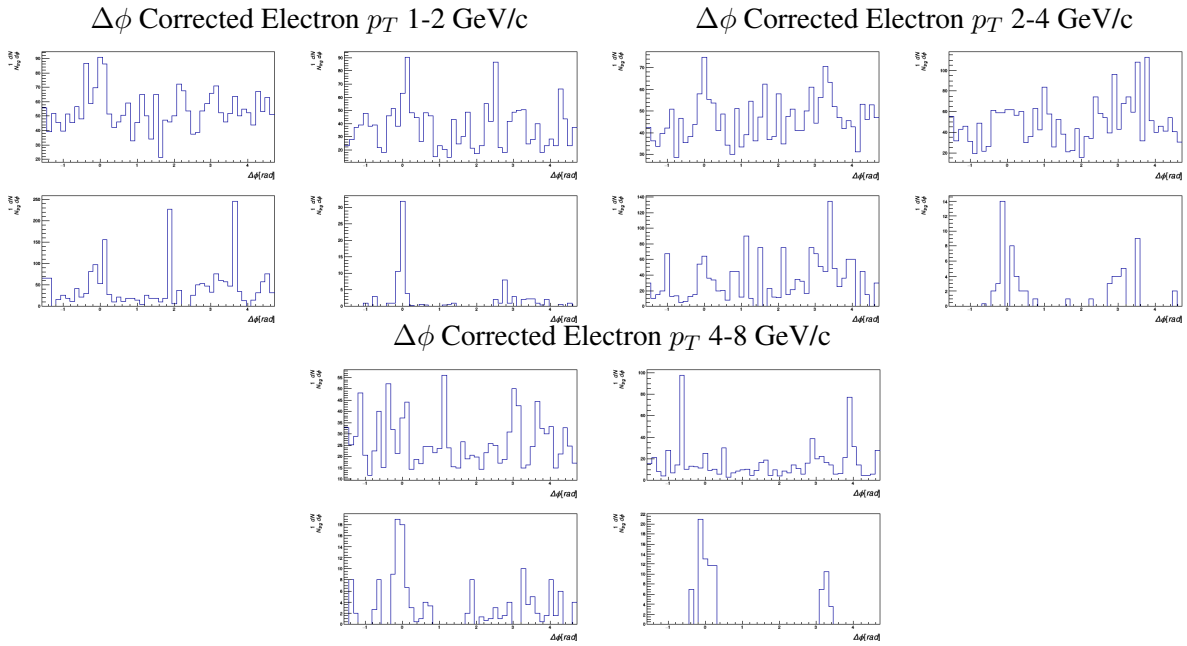

Figure 18: Corrected azimuthal correlations of candidate electrons, corrected for acceptance by mixed event analysis, and all other hadrons in that MB event. Each group represents a candidate electron p_T bin: 1-2 GeV/c (top left), 2-4 GeV/c (top right), and 4-8 GeV/c (bottom). Each individual plot in a group represents an associated hadron p_T bin: .3-1 GeV/c, 1-2 GeV/c, 2-4 GeV/c, 4-8 GeV/c. We have a huge bias that eclipses the double peak structure seen in the uncorrected azimuthal correlation plots. The coupling of low statistics and the geometric bias makes definitive statements about the structure of these plots difficult.

4.5 Full Jets and Charged Jets in the ALICE Detector

Our investigations into electron-hadron correlations served as an interim proxy for the ultimate goal of investigating fully reconstructed jets originating from bottom quarks. Jets are messy collections of collimated particles overlaid on top of all the many more uncorrelated particles in a given event. We must identify which particles belong to each jet by using a jet-finding algorithm. There are several currently in use with different benefits to each. We use a software package called FastJet[43] which contains the standard set of algorithms currently in use within ALICE and among the heavy ion community.

The particles composing jets are both charged and neutral. The charged particles are detected in both the TPC and the EMCal, the neutral particles are only detected in the EMCal. Since the EMCal does not cover the full azimuth, like the TPC, an analysis that investigates full jets (the collection of charged and neutral particles) is limited in acceptance to the EMCal's acceptance. One can investigate the charged

constituents of jets, the "charged" jets, using only information from the TPC. The charged jets are, however, missing information about the total energy and multiplicities of the full jet. Additionally, due to a phenomenon dubbed "subjettiness", the presence of one or more smaller jets in a larger jet, the charged jets may not always be adequate representatives of the full jets. This requires that comparisons of full jets and charged jets be subject to extra scrutiny.

Briefly, the algorithm used in our analysis is called the anti-kt algorithm. We calculate two distance measures, d_{ij} and d_{iB}, between the ith and jth particles and the ith particle and the beam. The ith particle is always the highest transverse momentum particle in the event. For each nearby smaller jth particle, if d_{ij} (Eq.2) is smaller than d_{iB} (Eq. 3) then it is added to the jet, otherwise the previously added particles are considered the whole jet and are removed from the event and the process is repeated. This identifies both full and charged jets. Figure 19 shows a visualization of how final jets are clustered.

$$d_{ij} = min(k_{ti}^{-2}, k_{tj}^{-2})\frac{\Delta_{ij}}{R^2} \tag{2}$$

$$d_{iB} = k_{tB}^{-2} \tag{3}$$

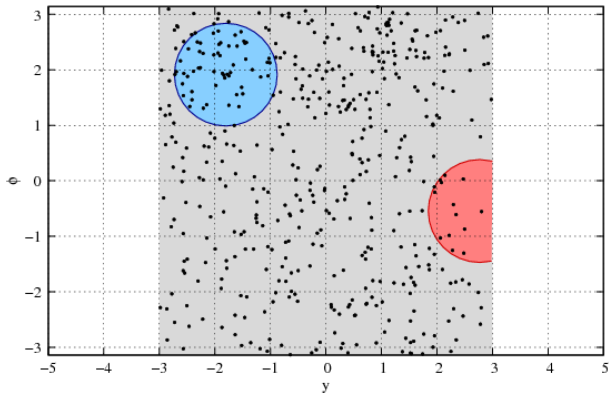

Figure 19: Finding jets using the FastJet algorithm looks roughly like this: Particles (dots) are clustered together and weighted by their momentum up to a certain resolution parameter (the blue and red circles). In charged jet analysis, only the momentum information from particles detected in the TPC is used. [43]

4.6 Electron-Led Jets and Their Away-Side Partners

Each jet is expected to contain a single high-p_T particle near the geometrical center of the jet called the leading particle. As the original parton from the collision fragments there is a primary decay, which

carries most of the parton's excess energy, that results in the leading particle. Around the leading particle are less energetic constituents with a spectrum of p_T like that shown in Figure 20. Investigations of the particle constituents of jets are of great interest [45] because they can provide insight into the fragmentation process and in-medium energy loss.

Each parton may produce different jets with different leading particles, however, certain leading particles can constrain the initial state parton. In the case of a bottom quark, the association of a jet with a leading electron implies a high likelihood that the primary decay associated with that jet is a bottom meson. By finding jets and constraining our selection to only those with a leading electron we are more likely to have a population of "bottom-jets". Since we use the EMCal as part of our electron identification, the tagged jets must lie within the EMCal acceptance. This greatly limits our population of bottom-jets and could be improved upon with a more robust electron identification method or with the inclusion of data from the DCAL, a detector opposing the EMCal, to extend the acceptance.

Hard-scattering of $q - \bar{q}$ and $Q - \bar{Q}$ pairs results in nearly back to back quark-led jets. This means that if we can identify a population of bottom jets in one direction with another jet near 180°, that pair of jets has a high likelihood of being from $Q - \bar{Q}$ scattering. We call these jets near-side and away-side respectively. At 180° (π rad) away from the near-side jet with a leading electron we expect to find an away-side jet with a wholly different fragmentation resulting in different constituents. It is these away-side constituents that we would like to study with this jet tagging method.

To select the away-side population of jets we first found all charged jets (jets without their neutral constituents) in the event. Then, we identified those jets with a leading electron and defined the axis of that jet as the azimuthal origin. We defined the away-side region as $\pi \pm \pi/4$ rads from the jet axis and identified jets within this region. This is shown in Figure 1. If there were multiple jets we selected the hardest, or highest p_T, jet and its away-side jet. This hopefully provides us with a minimally biased population of bottom jets on the away-side. For comparisons later on in the analysis we applied the same method for near-side jets with a leading hadron and collected a population of their away-side partners. This other population is most likely produced by light quarks(u,d,s) and gluons.

Present in the event are also particles from the underlying event, stray particles not belonging to a jet that contribute to the background. Since it is quite difficult to filter these particles out, corrections are

applied to the jet energy using an underlying event analysis [46].

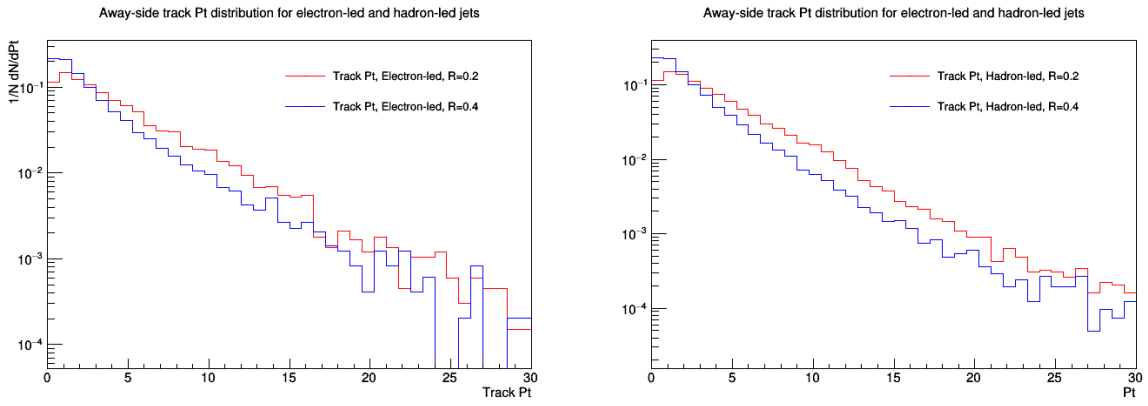

Figure 20: Transverse momentum spectrum for tracks within the electron-led (left) jets and the inclusive (right) jets for two different resolution parameters. The typical exponential form shows that in addition to the leading particle there are many other particles that are produced as the jet develops. Background particles are also present in the event, mixing with the jet.

4.7 Variables Used to Discriminate Light Quark Jets and Gluon Jets from Electron-led Jets

There have been some studies into discriminating light quark jets and gluon jets to provide a cleaner probe of QCD. These studies have mostly proceeded using geometric cuts to identify jets, e.g. gluon jets can be identified in a three-jet "Mercedes Logo" event. Then various jet variables are extracted and their spectra compared. In Monte-Carlo simulations, where the initial parton leading a jet is known, several jet variables have been identified as key discriminators; this is shown in Figures 21, 22. The variable that provides the best separation is the number of charged constituents in a jet. On the average quark jets have fewer charged constituents than gluon jets due to the gluon carrying a higher color charge. Further studies often construct multi-variate distributions involving the charged particle multiplicity [47].

We measured several variables in both the populations of tagged jets and inclusive jets. The jet momentum spectra were measured to show overall differences in the jet momenta between our populations. In addition, we measured the momentum spectrum of leading particles in each jet. Tagged bottom jets should impart most of their momentum to the leading particle, measured by way of the leading particle momentum fraction, which is defined as the ratio of the leading particle momentum to the total jet momentum. The jet area, or girth, measures the radial moment of the jet's constituents. This is a good

discriminator between light-quark and gluon jets due to the relative geometrical spread of each jet's respective constituents. Gluon jets tend to be wider than light quark jets due to many soft splittings as the jet evolves. This is also related to the color charge difference between quarks and gluons.

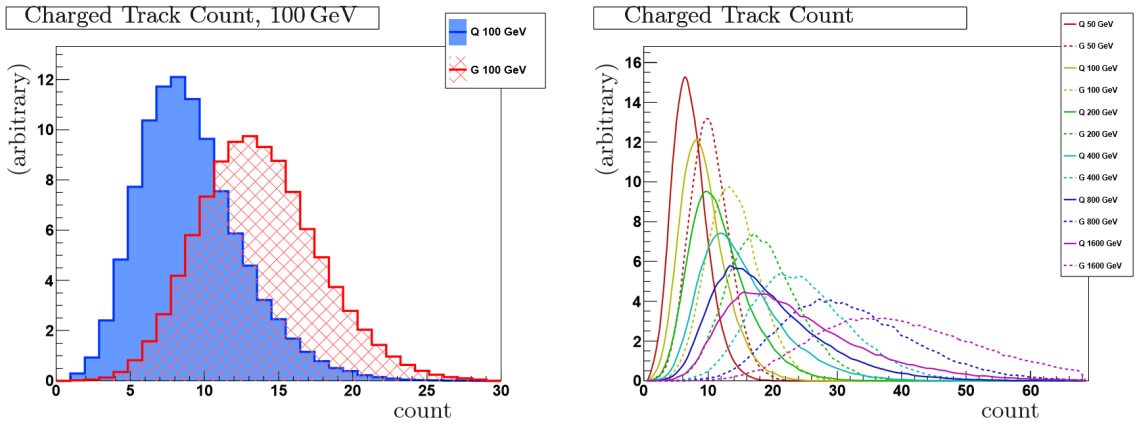

Figure 21: The charged particle multiplicity within light quark and gluon jets from PYTHIA simulations. Jets that originate from a quark are theorized to produce fewer particles than a jet coming from a gluon due to the difference in color charge. In every p_T range the gluon jets have more charged particles than the quark jets. However there is a significant amount of overlap between the distributions which limits this observable as a discriminating variable. [44]

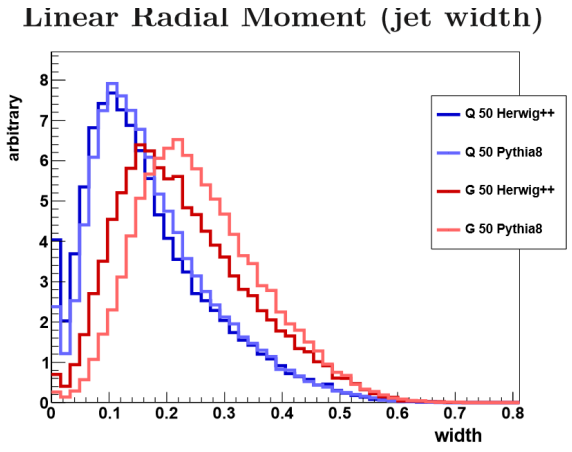

Figure 22: Linear radial moment or width (girth) of jets from light quark and gluon jets in PYTHIA and HERWIG. Jet girth is used with some success to discriminate light quark and gluon jets.[44]

The p_T spectra for electron-led and inclusive away side jets is shown in Figure 23. The sharp cut

below 10 GeV comes about because below 10 GeV we no longer consider the structures jets. Below each plot is the ratio of the electron-led to inclusive for this variable. Note that there is a possible enhancement in electron-led jets at high p_T and a possible suppression at low p_T.

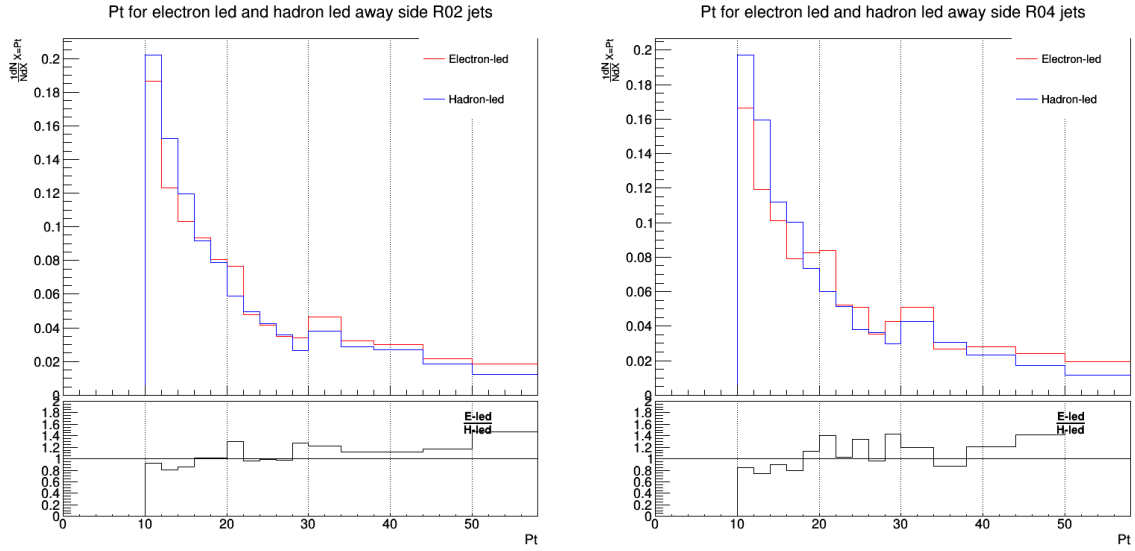

Figure 23: Transverse momentum (p_T) spectrum for R=0.2 jets (left) and R=0.4 jets (right) for away-side partners of electron-led and inclusive jets. Here there may be a hint for suppression of the ratio at low-p_T and a enhancement at high-p_T.

We considered only the leading particles within electron-led jets and inclusive jets and constructed their p_T spectra in Figure 24. Since our $>$ 10 GeV/c cut on jet p_T is still present we see very few low p_T leading particles; this makes sense because the leading particle represents a large fraction of the jet's p_T. Below each plot is the ratio of electron-led to inclusive jets in the distribution. As with the jet p_T spectrum, we see a stronger enhancement at high p_T for electron-led jets. Among the variables we studied, this one showed the greatest difference between the populations. Since the inclusive jets will mostly originate from light quarks and gluons they will either be softer(lower p_T) on average or more diffuse energetically. In either case they will impart less momentum to the leading particle than in the electron-led jets.

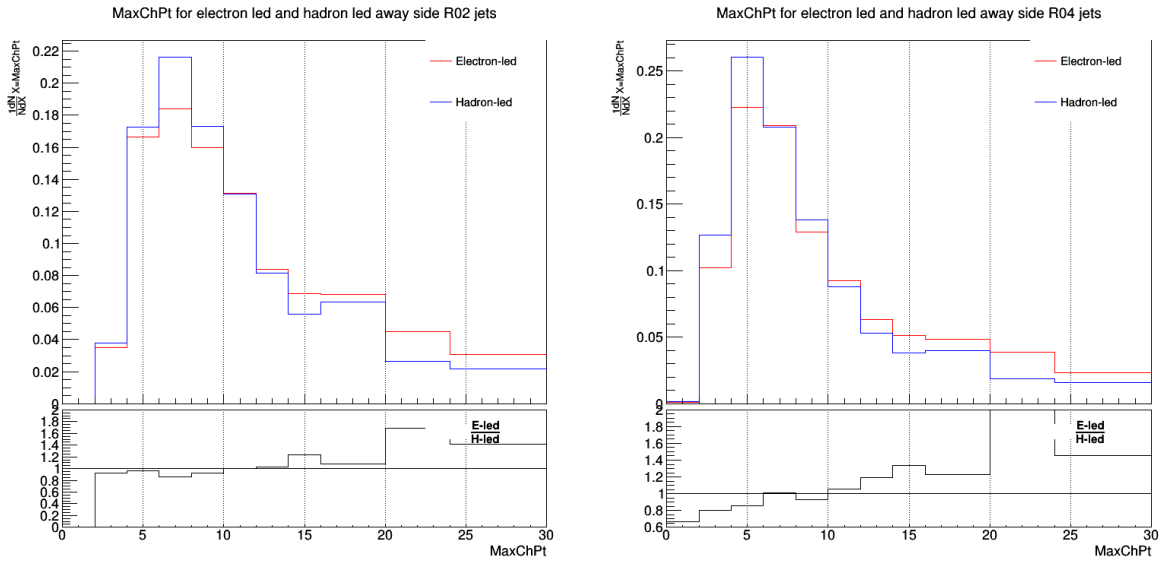

Figure 24: Transverse momentum (p_T) spectrum for the jet constituent with the largest p_T within its own jet with R=0.2 (left) and R=0.4 (right) for away-side partners of electron-led and inclusive jets. Here there may be another hint for suppression of the ratio at low-p_T and a enhancement at high-p_T as seen in the raw p_T spectrum.

The charged particle multiplicity was measured for the electron-led and inclusive away-side jets and is shown in Figure 25. Below each plot is the ratio of electron-led to inclusive jets in this distribution. We see the the ratio is close to unity across the p_T range until statistics become too low make any definitive statements.

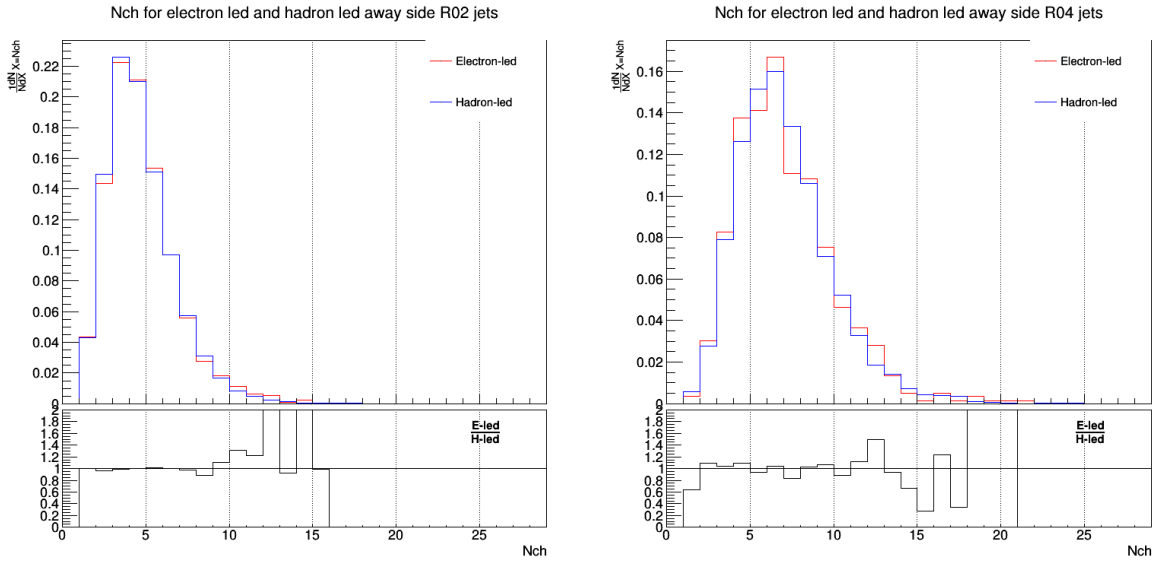

Figure 25: Charged particle multiplicities for away-side partners of primary electron-led and inclusive jets with resolution parameters of R=0.2 (left) and R=0.4 (right). The charged particle multiplicity is an important observable for discriminating light quark and gluon jets. In each we observe a similar distribution and a ratio that is close to unity.

A high p_T jet is expected to produce particles within a tighter cone around the jet axis and impart a larger momentum fraction into its leading particle; thus we expect bottom jets to have a leading particle momentum fraction close to one. We measured the momentum fraction for the leading particle in electron-led jets and inclusive jets in Figure 26. Below each plot is the ratio of electron-led to inclusive jets. We find this ratio to be close to unity across the p_T range, showing significant variation. The peak at 1 in R=0.2 jets is most likely due to individual particles being identified as jets due to the small R.

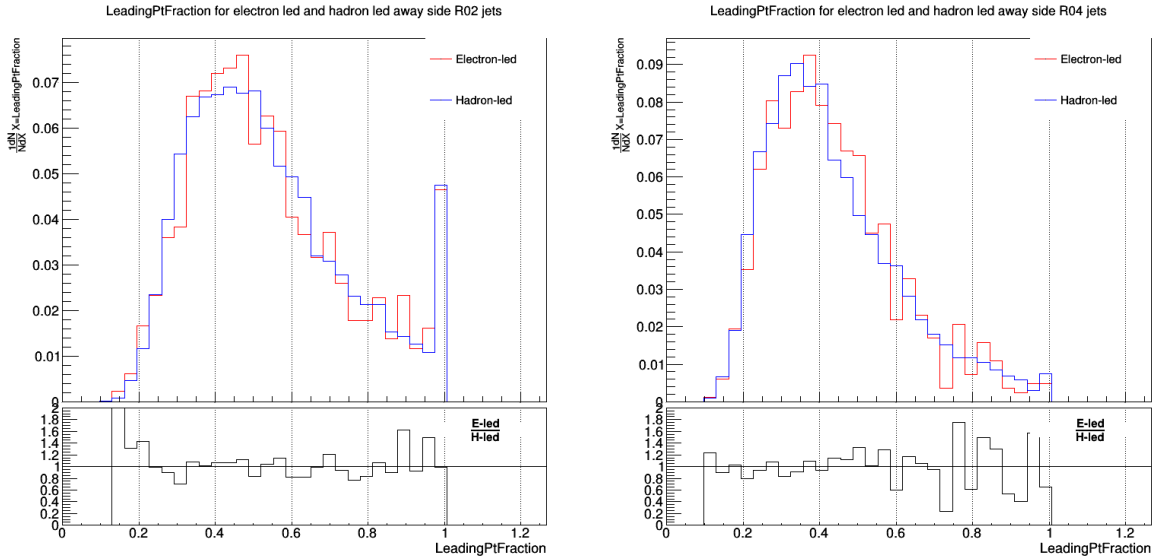

Figure 26: Leading p_T fraction for R=0.2 (top) and R=0.4 (bottom) for away-side partners of electron-led and inclusive primary jets.

The momentum-weighted spread of the constituents within a jet is called the jet area, or girth. We measured the girth for electron-led and inclusive jets in Figure 27. Below each plot is the ratio of electron-led to inclusive jets. We see that the ratio is close to unity across the range of jet girth. We do not observe a significant difference in this variable for our tagged bottom jet population compared to the inclusive jet population.

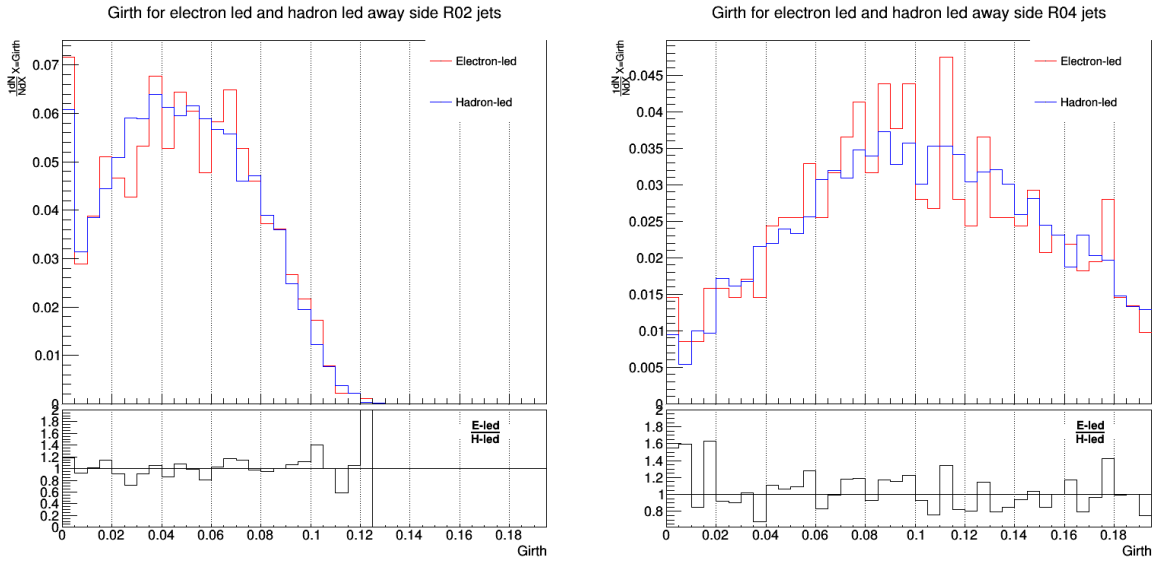

Figure 27: Jet girth for R=0.2 (left) and R=0.4 (right) of the away-side partners of electron-led and inclusive primary jets. Both plots remain around unity in the ratio of the two jet populations.

5 Discussion

Our goal for this analysis was to find evidence for differences in the away-side jet constituent distributions when the near-side jet is tagged with an electron, suggesting that it came from a bottom quark hard scattering. We investigated electron-hadron azimuthal correlations by identifying high p_T electrons using three detectors. We found a relatively pure sample of electrons using fairly stringent cuts on all the PID detectors. From this sample we identified potential background contamination from photon conversions inside the detector structure as well as from hadrons present in the event. There were a low number of electrons from photon conversions in our sample mostly due to the requirement for high momentum electrons. Hadron contamination was also low.

With our electron sample we correlated each with the hadrons in the remaining event. From this we constructed the azimuthal distributions with respect to the electron axis and revealed the characteristic double peak structure. In order to correct for detector acceptance biases we use a mixed event analysis to generate uncorrelated azimuthal distributions for each electron. This distribution should be uniform if there are no acceptance biases. However, our mixed event azimuthal distributions showed a large bias

due to the requirement that our electron sample lie within the EMCal acceptance. We thus produced a corrected azimuthal distribution by subtracting the mixed event distribution, resulting in a structure that poorly reflects the one found in the raw correlations. We anticipate that removing the EMCal requirement, and including a 2π azimuthal acceptance, would reduce this bias, but it would also reduce the efficiency of the electron identification. In order to estimate the increase in statistics necessary to produce a 5% significance we take the average counts in a correlation plot to be 30,000 with a corresponding uncertainty of $\sqrt{30,000} = 173$. For our corrected correlations we add the same uncertainty from the mixed event analysis for a total uncertainty of 346. The near side peak to background difference is 80 counts. In order to produce a significant result, we need a near side peak to background difference of 0.95(346) $\sim$ 700 counts. Thus, an appropriate sample for this analysis must contain more than 8.5 times the current statistics.

We then investigated fully reconstructed jets that have a high p_T electron leading them and compared them to inclusive jets not tagged with an electron (presumably hadron-led). We expected that the electron-led jets would represent a population produced from hard-scattered bottom quarks and the inclusive jets represent light quark and gluon partons. We measured five variables in order to discriminate electron-led and inclusive jets, constituent p_T, leading particle p_T, charged particle multiplicity within jets, leading momentum fraction, and girth. In the constituent p_T and leading particle p_T distributions we saw some hints for enhancement at high p_T. The remaining variables showed little variation between the two populations.

Overall, we developed a set of PID and kinematic cuts that produce a relatively pure sample of electrons, albeit with low statistics. This population would increase with a larger sample of events. Increasing the acceptance of PID detectors could also improve both the statistics and reduce the bias imposed by using the EMCal for electron identification. Now that the ALICE DCal is fully installed, future analyses could use the DCal to provide somewhat greater acceptance as well as to analyze the away-side jets as full jets. The variables used to compare electron-led and inclusive jets, while useful in discriminating light quark and gluon jets with Monte-Carlo generators, have been shown to be not effective for our analyzed data. Future analyses will need to devise new variables with greater discriminatory power. Ultimately we hope that studies like these can shed light on the differences between quark and gluon-led jets, en-

abling us to develop a better understanding of the fundamental theory of strong interactions, quantum chromodynamics.

References

[1] Riordan, M. SLAC, The Discovery of Quarks (1992).

[2] Adcox, K. et al. (PHENIX Collaboration), Suppression of Hadrons with Large Transverse Momentum in Central $Au + Au$ Collisions at $\sqrt{s_{NN}}$=130G_{eV} Phys. Rev. Lett. 88, 022301 (2001).

[3] Vernet, R. for the ALICE Collaboration, Soft Probes of the Quark-Gluon Plasma with ALICE at LHC (2009). [arXiv:0906.1171 [nucl-ex]]

[4] Salgado, Carlos A., Hard Probes of the Quark Gluon Plasma in Heavy Ion Collisions AIP Conf.Proc. 1441 (2012). [arXiv:1109.4082 [hep-ph]]

[5] Ali, Ahmed et al., Jets and QCD: A Historical Review of the Discovery of the Quark and Gluon Jets and its Impact on QCD Eur.Phys.J. H36 (2011). [arXiv:1012.2288 [hep-ph]]

[6] Andersson, Bo et al., Parton Fragmentation and String Dynamics Phys.Rept. 97 (1983).

[7] Qin, Guang-You et al., Jet quenching in high-energy heavy-ion collisions Int.J.Mod.Phys. E24 (2015). [arXiv:1511.00790 [hep-ph]]

[8] PHENIX Collaboration Adcox, K. et al., Suppression of hadrons with large transverse momentum in central Au+Au collisions at $\sqrt{s_{NN}}$ = 130 GeV Phys.Rev.Lett. 88 (2002). [arXiv:nucl-ex/0109003]

[9] STAR Collaboration Abelev, B.I. et al., Studying Parton Energy Loss in Heavy-Ion Collisions via Direct-Photon and Charged-Particle Azimuthal Correlations Phys.Rev. C82 (2010). [arXiv:0912.1871 [nucl-ex]]

[10] Nagle, J.L. et al., Quarkgluon plasma at the RHIC and the LHC: perfect fluid too perfect? New Journal of Physics, Volume 13 (2011).

[11] (STAR) J. Adams et al., Evidence from d+Au Measurements for Final-State Suppression of High-p_T Hadrons in Au+Au Collisions at RHIC Phys. Rev. Lett. 91, 072304 (2003).

[12] (ALICE Collaboration) Abelev, Betty et al., Measurement of electrons from semileptonic heavy-flavour hadron decays in pp collisions at $\sqrt{s}$ = 7 TeV - Phys.Rev. D86 (2012) 112007 arXiv:1205.5423 [hep-ex] CERN-PH-EP-2012-131

[13] Ali, Ahmed et al., Jets and QCD: A Historical Review of the Discovery of the Quark and Gluon Jets and its Impact on QCD Eur.Phys.J. H36 (2011). [arXiv:1012.2288 [hep-ph]]

[14] Nattrass, Christine, Jet quenching: an iconic result revisited [arXiv:1801.09131 [nucl-ex]]

[15] CMS Collaboration Chatrchyan, Serguei et al., Identification of b-quark jets with the CMS experiment JINST 8 (2013). [arXiv:1211.4462 [hep-ex]]

[16] Goncalves, Dorival et al., Distinguishing b-quark and gluon jets with a tagged b-hadron Phys.Rev. D93 (2016). [arXiv:1512.05265 [hep-ph]]

[17] CDF Collaboration Acosta, D. et al., Heavy flavor properties of jets produced in $p\bar{p}$ interactions at $\sqrt{s}$ = 1.8 TeV Phys.Rev. D69 (2004). [arXiv:hep-ex/0311051]

[18] Cacciari, Matteo et al., The Anti-k(t) jet clustering algorithm JHEP 0804 (2008). [arXiv:0802.1189 [hep-ph]]

[19] Qin, Guang-You et al., Jet quenching in high-energy heavy-ion collisions Int.J.Mod.Phys. E24 (2015). [arXiv:1511.00790 [hep-ph]]

[20] Kormilitzin, Andrey et al., On the Nuclear Modification Factor at RHIC and LHC Nucl.Phys. A860 (2011). [arXiv:1011.1248 [hep-ph]]

[21] Zhang, Bin et al., Nuclear modification of heavy quark fragmentation function and J / psi production in ultrarelativistic heavy ion collisions Phys.Lett. B546 (2002). [nucl-th/0205064]

[22] J. Adams et al. (STAR Collaboration), Evidence from d+Au Measurements for Final-State Suppression of High-p_T Hadrons in Au+Au Collisions at RHIC Phys. Rev. Lett. 91, 072304 (2003).

[23] Renk, Thorsten, Jet quenching and heavy quarks J.Phys.Conf.Ser. 509 (2014). [arXiv:1309.3059 [hep-ph]]

[24] Martinez, Gines, Advances in Quark Gluon Plasma (2013). [arXiv:1304.1452 [nucl-ex]]

[25] Pasechnik, Roman et al., Phenomenological Review on QuarkGluon Plasma: Concepts vs. Observations, Universe 3 (2017). [arXiv:1611.01533 [hep-ph]]

[26] Breskin, Amos (ed.) and Voss, Rudiger (ed.) (CERN), CERN Large Hadron Collider : Accelerator and Experiments, Volume 1 (2009).

[27] Breskin, Amos (ed.) and Voss, Rudiger (ed.) (CERN), CERN Large Hadron Collider : Accelerator and Experiments, Volume 2 (2009).

[28] Fabjan, Christian Wolfgang et. al., ALICE trigger data-acquisition high-level trigger and control system: Technical Design Report, Technical Design Report ALICE (2004).

[29] Technical design report of the ALICE Inner Tracking System, CERN / LHCC 99 12 ALICE TDR 4 (1999).

[30] Technical design report of the ALICE Time Projection Chamber, CERN / LHCC 2000 001 ALICE TDR 7 (2000).

[31] Cortese, P, ALICE transition-radiation detector : Technical Design Report (2001).

[32] ALICE Collaboration, ALICE Electromagnetic Calorimeter Technical Design Report (2008).

[33] Gallicchio, J. & Schwartz, M. D. Journal of High Energy Physics (2011). [arXiv:1104.1175 [hep-ph]]

[34] OPAL Collaboration, Alexander et. al., A comparison of b and uds quark jets to gluon jets Zeitschrift fr Physik C Particles and Fields (1995).

[35] Tasevsky, M. Differences between Quark and Gluon jets as seen at LEP (2001). [arXiv:hep-ex/0110084]

[36] Gallicchio, J. & Schwartz, M. D. Quark and Gluon Tagging at the LHC Phys.Rev.Lett. 107 (2011). [arXiv:1106.3076 [hep-ph]]

[37] B. Andersson et al., "Parton Fragmentation and String Dynamics", Phys. Rep. 97(2 & 3), 31145 (1983).

[38] CMS Collaboration Search for supersymmetry in multijet events with missing transverse momentum in proton-proton collisions at 13 TeV Phys. Rev. D 96, 032003 (2017).

[39] Bertella, C. Probing top quark and Higgs boson production in multi-jet events at the LHC with the ATLAS detector Marseille, CPPM, Marseille, CPPM, (2013).

[40] M. Connors, C. Nattrass, R. Reed, and S. Salur, Review of Jet Measurements in Heavy Ion Collisions (2017). [arXiv:1705.01974]

[41] Ali, A. & Kramer, G. Jets and QCD: A Historical Review of the Discovery of the Quark and Gluon Jets and its Impact on QCD Eur. Phys. J. H 36, 245 - 326 (2011). [arXiv:1012.2288 [hep-ph]]

[42] Tannenbaum, M. J. Review of hard scattering and jet analysis PoSCFRNC2006:001, (2006). [arXiv:nucl-ex/0611008]

[43] M. Cacciari, G.P. Salam and G. Soyez, Eur.Phys.J. C72, (2012). 1896 [arXiv:1111.6097]

[44] Gallicchio, Jason et al., Quark and Gluon Jet Substructure JHEP 1304 (2013). [arXiv:1211.7038 [hep-ph]]

[45] Zenz, Seth, Understanding Jet Structure and Constituents: Track Jets and Jet Shapes at ATLAS, ATL-PHYS-PROC-2010-126, ATL-COM-PHYS-2010-937 (2010).

[46] CMS Collaboration (Khachatryan, Vardan et al.), Measurement of the underlying event activity using charged-particle jets in proton-proton collisions at sqrt(s) = 2.76 TeV, JHEP 1509 (2015). [arXiv:1507.07229 [hep-ex]]

[47] Gallicchio, Jason et al., Quark and Gluon Jet Substructure, JHEP 1304 (2013). [arXiv:1211.7038 [hep-ph]]